AIAA SciTech Forum
6-10 January 2020, Orlando, FL
AIAA Scitech 2020 Forum

10.2514/6.2020-0097

Streamwise Evolution of Turbulent Boundary Layer Response to Active Control Actuator

Mitchell Lozier[1], Flint O. Thomas[2], Stanislav Gordeyev[3]
University of Notre Dame, Notre Dame, IN, 46556

In these studies, a plasma based active flow control device was used to introduce periodic motions into the wake region of the turbulent boundary layer. The boundary layer Reynolds number was low enough, $Re_\tau = 683$ that no natural large-scale structure was present. Through actuation, a synthetic large-scale periodic shear-layer-like structure was introduced into the boundary layer, and the boundary layer response to this synthetic structure at various wall-normal and streamwise locations downstream of the actuator was studied using a single hot-wire. Due to the periodic nature of the forcing, a phase-locked triple Reynolds decomposition of velocity was used to analyze the data. The evolution of near-wall residual turbulence modulated by the synthetic structure in the inner and log regions of the boundary layer was analyzed. The dynamics of the synthetic structure and small-scale structures were then quantified using several modulation coefficients. These modulation coefficients show a strong positive correlation in the inner and log region of the boundary layer. The evolution of the synthetic large-scale structure and its modulating effect on the near-wall turbulence at several streamwise locations was described.

I. Introduction

In recent years, the large-scale structures (LSS) in turbulent boundary layers (TBL) and their effect on the technologically relevant flow properties (friction drag, noise, aero-optical distortions, flow separation etc.) have been extensively investigated [1,2,3] and it was demonstrated that the dynamics of LSS and near-wall small-scale turbulence is correlated [3,4]. Furthermore, the influence of the LSS in TBL dynamics was shown to increase with Reynolds number [3].

In canonical boundary layers, thin shear layers, separating low-speed and high-speed regions (so-called uniform momentum regions), have been observed and studied in the last few years [5,6]. These thin shear layer structures, combined with the low momentum flow underneath them, are believed to be parts of a coherent structure, also known as the Attached Eddy. A more recent investigation of adverse pressure gradient TBLs demonstrated that the local flow physics is largely dominated by an embedded shear layer associated with the inflectional instability of the outer mean velocity profile inflection point

[1] Graduate student, Department of Aerospace and Mech. Eng AIAA Student member.
[2] Professor, Department of Aerospace and Mech. Eng., AIAA Associate Fellow
[3] Associate Professor, Department of Aerospace and Mech. Eng., AIAA Associate Fellow

[7]. Using scaling laws developed for free shear-layers but applied to the adverse pressure gradient (APG) TBL, profiles of mean velocity and turbulence quantities exhibited a remarkable collapse. The generic applicability of the embedded shear layer scaling was demonstrated by collapsing multiple APG turbulent boundary layer data sets from the AFOSR-IFP-Stanford Conference compiled by Coles and Hirst [8]. Further support for the influence of the shear layer structure on the near-wall TBL dynamics was recently provided by a study demonstrating that the presence of a free shear layer just outside a TBL has a significant effect on the near-wall bursting/sweep events [9].

Collectively, the results described above strongly suggest that embedded shear layers are a generic feature of all TBLs irrespective of whether or not the mean velocity profile is inflectional. Although more apparent in APG boundary layers with inherent inflectional mean velocity profiles, transient and non-localized inflectional instabilities could well account for the enhancement of outer large-scale boundary layer structure that has been documented in previous studies of high Reynolds number zero pressure gradient TBLs. These shear-layer-like structures likely play an important role in determining LSS dynamics and ultimately in the global properties of the TBL.

An intriguing aspect of the presence of shear layers in the TBL is that they are very amenable to control. The ability to independently control outer layer LSS in the TBL offers new possibilities for uncovering their underlying dynamics. This aspect has been largely unexplored and most studies and models regarding the relationship between the small- and the large-scale structures deal with natural un-manipulated TBLs and apply various conditional-averaging techniques to study their interactions [4]. Only a small number of studies investigated modifying the LSS directly. In [10] an oscillating vertical plate was used to introduce a controlled traveling wave into the log-region of the boundary layer, and triadic interactions between the induced periodic structure and various scales in the boundary layer were studied. In [9] the turbulent boundary layer was externally forced by a shear layer and the turbulence inside the boundary layer was found to be both amplified and modulated by the external forcing.

Inspired by the results in [9], in this paper, active flow control is used to introduce periodic disturbances into the wake region of the turbulent boundary layer. The boundary layer Reynolds number is low enough, so there is no natural large-scale structure present. By introducing periodic distortions, a synthetic large-scale structure was introduced into the boundary layer. In [11] it was demonstrated that this periodic active flow control had sufficient authority within the boundary layer to produce a synthetic large-scale structure with a measurable modulation effect on the near wall small-scale structures.

In this paper, we further explore the interaction between the synthetic large-scale structure, introduced by the actuator, and the near-wall turbulence. Specifically, the evolution of the large-scale structure was analyzed at several streamwise locations. To quantify the near-wall response to the convecting large-scale structure, two-point correlation analysis was performed, and various correlation functions were computed and analyzed at the same streamwise locations downstream of the actuator.

II. Experimental Set-Up

All of the experimental results presented in this paper were obtained using the 2' x 2' subsonic in-draft wind tunnel facility in the Hessert Laboratory at the University of Notre Dame. The overall dimensions of the tunnel test section are 2' x 2' x 7'. For this experiment, a boundary layer development plate 2 meters long with a roughness element attached to the leading edge was installed in the tunnel. A constant temperature anemometer (CTA) with a single boundary layer hot-wire probe (Dantec Type 55P15) with 5 μm diameter and l = 1.5 mm length ($l^+ = 26$) was used to collect time series of the streamwise velocity component. A computer controlled traversing stage was inserted through the top wall of the tunnel along the midpoint of the tunnel span to allow the hot wire anemometer probe to traverse the test section and make measurements at different wall normal or y-locations. The plasma actuator device, as described below, was attached to the top side of the boundary layer development plate at a fixed streamwise location of 140 cm from the leading edge of the boundary layer development plate. The hot wire probe and plasma actuator are shown in Figure 1. The hot wire probe traverse system was also adjustable in the streamwise direction and was positioned at four streamwise or x-locations measured downstream of the plasma actuator trailing edge, in order to measure the TBL response at multiple locations. The locations selected for this experiment were 51 mm, 102 mm, 170 mm, and 272 mm, which correspond to 1.5δ, 3δ, 5δ, and 8δ, respectively, based on the experimentally determined boundary layer thickness. A set of representative turbulent boundary layer characteristics were measured at the downstream location of 3δ using the hot wire probe. These parameters are summarized in Table 1 for reference. The skin friction velocity u_τ was found using the Clauser method. In all of the experiments described below, the tunnel free stream velocity was 7 m/s.

Table 1. Turbulent boundary layer parameters at $x = 3\delta$

δ	U_∞	u_τ	C_f	H	Re_θ	Re_τ
33.2 mm	6.95 m/s	0.304 m/s	0.0039	1.368	1,770	683

A plasma-based Active Large-Scale Structure Actuator (ALSSA) device was used in this experiment to modify the dynamics of the boundary layer. The plasma actuator was supported in the tunnel by two vertical NACA0010 airfoil supports which were 4 mm thick and had a height of H = 21 mm or 0.6δ. The plasma actuator was W = 10 cm wide in the spanwise direction and the plasma actuator length in the streamwise direction was L = 52 mm. The actuator plate was made of a 2 mm thick sheet of Ultem dielectric polymer. The leading edge of the actuator plate was rounded, and the trailing edge was tapered to reduce the separation region behind the trailing edge of the plate. The alternating current (AC) dielectric barrier discharge plasma formed on the actuator was produced using a high voltage AC source which consisted of a function generator, power amplifiers and a transformer [12]. Electrodes on the top and bottom of the actuator were connected to the high voltage AC source which provided a 40kV peak-to-peak sinusoidal waveform excitation to the electrodes at a frequency of 4 kHz. At this high actuation frequency, the plasma operates in a quasi-steady mode, essentially creating a spanwise-uniform steady jet. To introduce periodic forcing, a fifty percent duty cycle was imposed on the waveform, with a repetition frequency, f_p = 50 Hz.

A pitot probe was also inserted upstream of the plasma actuator through the side wall of the tunnel to measure the free stream velocity of the tunnel in order to calibrate the hot wire probe. Hot wire voltages, pitot probe pressure transducer voltages and the output of the function generator to the ALSSA device were recorded simultaneously in every test. The data was sampled at f_s = 30 kHz which corresponds to $\Delta t^+ = (1/f_s)u_\tau^2/\nu = 0.2$ for a total period of 150 seconds, or about 25,000 δ/U_∞ in each test. The hot wire probe was conditioned by a low pass filter with a cutoff frequency of 14 kHz to eliminate aliasing effects.

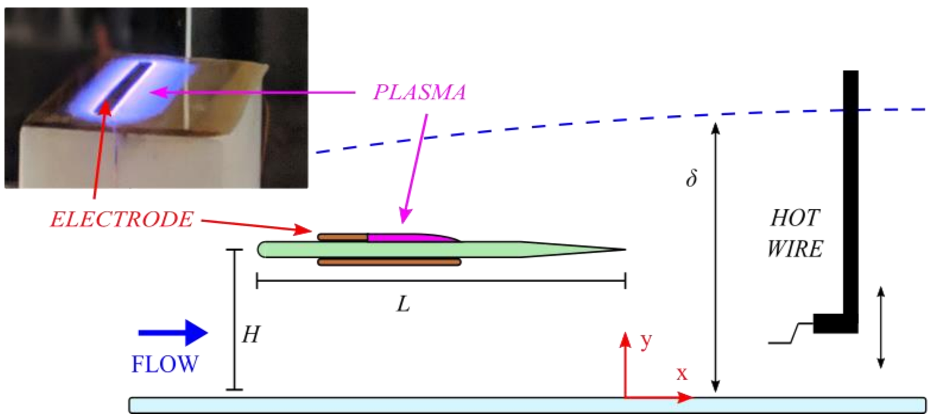

Figure 1. Schematic of experimental set-up with picture of plasma-based ALSSA.

III. Data Reduction

The data reduction for the experiment started with converting the measured voltages from the hot wire probe into velocities. The wind tunnel was calibrated by running at several free stream velocities between zero and nine meters per second while recording both the voltage from the pitot probe pressure transducer and the hot wire probe while the hot wire was positioned in the free stream. The voltage measured from the pitot probe pressure transducer is proportionally related to the physical dynamic pressure by a calibration constant that was experimentally determined before the experiments were conducted. The free stream velocity was calculated from this dynamic pressure using a 3rd-order polynomial. These velocity time series were then digitally low-pass filtered with a cutoff frequency of 4 kHz to eliminate electronic noise associated with the high voltage AC source supplying the actuator. After the hot wire voltages were converted to velocities and filtered, the time mean, U, and root mean square (RMS) of the velocity, u_{rms} were calculated at every location using standard methods. Since the actuator introduced periodic forcing into the flow, it is convenient to phase-lock the results to the actuation frequency. To do so, a triple phase-locked Reynolds decomposition of the velocity was considered, as shown in Equation 1 where u is the instantaneous velocity, U is the time mean component of velocity, $\tilde{u}$ is a phase dependent or modal velocity component, u' is a residual fluctuating turbulent component, φ is the phase, defined by the relationship in Equation 2, and n is the number of realizations as described below

$$u(y,t) = U(y) + \tilde{u}(y,\varphi) + u'(y,\varphi,n) \tag{1}$$

$$\varphi = \left(\frac{t_n}{T_p} - n\right) 2\pi \tag{2}$$

Here t_n is a time in the n^{th} realization which is related to the phase angle, φ, by the period of the forcing repetition cycle. $T_p = 1/f_p$. The output of the function generator was used to ensure the data was phase locked with the repetition cycle of the plasma. These n realizations are then ensemble averaged to find the modal component of velocity as a function of the phase angle. The remaining fluctuating component of the velocity, u' was used to quantify an ensemble-averaged RMS of the residual fluctuating turbulence shown in Equation 3.

$$u'_{rms} = (\langle [u'(y,\varphi,n)]^2 \rangle_n)^{\frac{1}{2}} \tag{3}$$

Here the square brackets denote ensemble averaging over all realizations. Later we will refer to this quantity as a residual turbulence level. The phase-averaged mean can be removed from the residual turbulence level to define local changes in residual turbulence.

IV. Results

The mean velocity of the boundary layer in inner unit scaling is presented in Figure 2, left. The universal fit for the log-region, $U^+ = 1/\kappa \ln(y^+) + C$ with values of κ = 0.385 and C = 4.1 is also plotted in Figure 2. The buffer and viscous sublayer can be seen for $y^+ < 30$. The log-region of the boundary layer is present between $30 < y^+ < 200$. The geometric center of the log-region is approximately $y^+ \sim 90$, close to the expected value of $y^+_{OL} \sim 3.9 Re_f^{1/2} = 102$ [2, 13]. The fluctuating component of the velocity, u'^2_{rms}, in inner unit scaling is shown in Figure 2, right. The maximum turbulence level occurs at $y^+ = 15$, with the value of $u'^2_{rms}/u^2_\tau \sim 6.6$.

The premultiplied energy spectrum of the canonical boundary layer is presented in Figure 3, left. Only the inner peak at $y^+ \sim 15$ and $\lambda^+ \sim 800$ is present in the energy spectra. The outer peak is essentially absent since in this experiment because Re_τ is relatively low. In Figure 3, right the narrow peak near $y^+ \sim 500$ and $\lambda/\delta \sim 3.7$ is a periodic localized structure that results from the synthetic large-scale structure being produced by the ALSSA device when it is turned on.

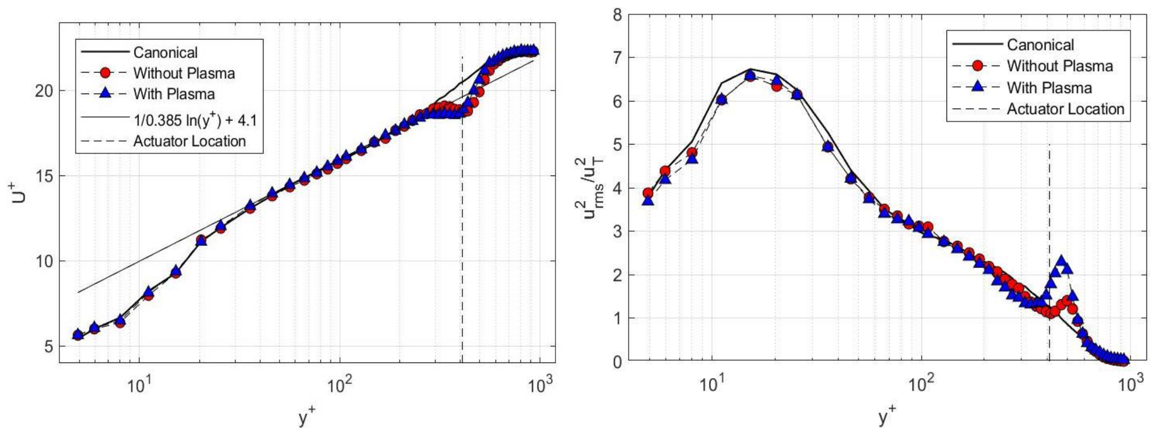

Figure 2. Mean velocity (left) and normalized variance (right) profiles for the canonical boundary layer, plasma off, and periodic plasma on cases at $x = 3\delta$ downstream of plasma actuator. The actuator location is indicated by a vertical dashed line.

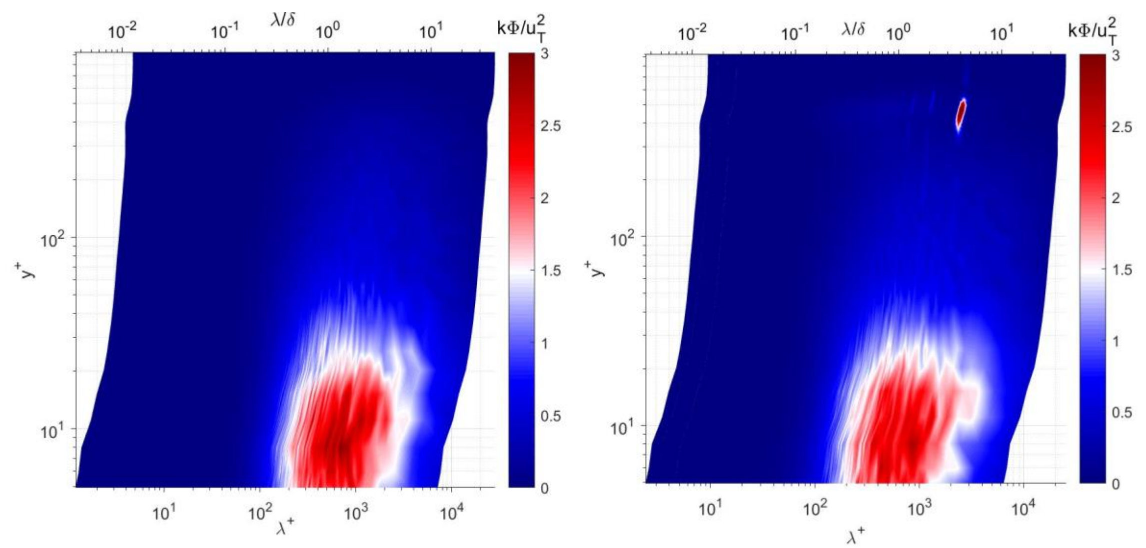

Figure 3. Pre-multiplied energy spectrum in the inner units for the canonical boundary layer (left) and for the plasma-on case (right) at $x = 3\delta$ downstream of plasma actuator.

As discussed before, ALSSA was placed inside of the boundary layer at a wall normal y-position of 0.6δ or y^+_{act} = 410 away from the wall to measure the effect it had on the boundary layer. The mean velocity profiles, U(y), in the boundary layer at $x = 3\delta$ for the case of plasma off and the periodic plasma on are presented in Figure 2, left, along with the velocity profile for the undisturbed canonical boundary layer. The mean velocity profiles for the canonical and plasma on and off cases show good agreement for $y^+ < 250$. As the plate is located approximately at $\mathrm{y}^+_{\mathrm{act}}$ = 410, indicated as a vertical dashed line in Figure 2, left, the velocity profile shows an actuation-related velocity deficit in the wake region of the boundary layer between $200 < \mathrm{y}^+ < 600$. Profiles of the normalized variance of the fluctuating velocity at x = 3δ for plasma off and plasma on cases are presented in Figure 2, right. The boundary layer statistics seem unchanged by the plasma actuator near the wall for $y^+ < 200$. For the plasma off case, the small local increase in the turbulence levels, related to the turbulent wake downstream of the plate, can be observed between $400 < y^+ < 600$. Note that the local increase in turbulence levels occur only above the plate, while the variance is slightly suppressed below the plate. When the periodic plasma is turned on, the turbulent peak downstream of the plate widens and is almost doubled in its intensity. Still, most of the increases in the turbulent intensity happens above the plate.

While the modifications of the mean and fluctuating velocity profiles in the wake region are a good indication that the actuator has authority in the boundary layer [11], the characterization of the interaction of a synthetic large-scale structure, introduced by the plasma actuator with the small-scale turbulent structures near the wall is of a primary interest.

Two-point correlation functions calculated using Equation 5 were computed to analyze the correlation between velocities at different heights within the boundary layer. Here y is the correlated velocity location, y' are all points measured within the boundary layer thickness, and τ is a time delay in seconds.

$$R(y, y', \tau) = \frac{\overline{u(y,t)\, u(y', t+\tau)}}{\sigma_{u(y)}\, \sigma_{u(y')}} \tag{5}$$

The results for two streamwise locations of $x/\delta = 3$ and 5 with $y = 0.6\delta$ are presented in Figure 4. In Figure 4 there are regions of non-zero correlation that extend from the actuator location all the way down to the wall. The positive correlation regions near the wall show a negative time delay, implying that fluctuations near the wall are leading fluctuations at the actuator location. It can also be seen that this delay time as well as the correlation intensity are changing as the measurement location moves further downstream. As the large-scale motions convect downstream, the changes in velocity near the wall are becoming more in phase and more strongly correlated with the large-scale velocities at the actuator location.

In Figure 5 the modal velocities for two downstream locations have been plotted in phase space as described in the data reduction section. There is a very strong modal velocity component at the actuator location, which is expected. This component looks to be relatively constant in size and shape moving downstream. There is also a region of weaker modal velocity that extends towards the wall. The alignment of this component relative to the modal velocity at the actuator location does seem to be changing and growing in strength. Because of the periodic nature of mapping quantities in phase it is not straightforward to compare the modal velocity at different measurement locations as demonstrated in Figure 5. In Figure 6, left, the modal velocities at the actuator location for three downstream locations have been plotted to show that it is hard to understand the streamwise evolution of the modal velocity by looking at the quantities in phase.

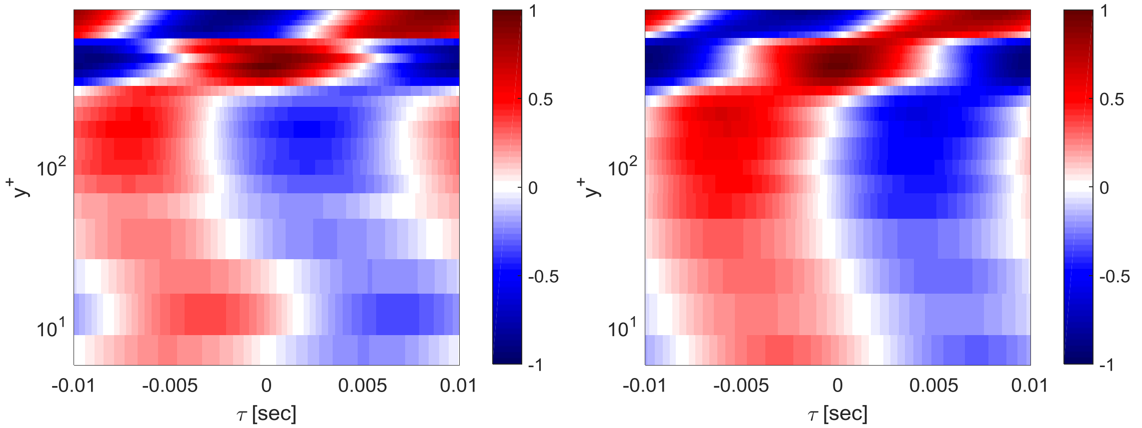

Figure 4. Normalized correlation with velocity at $y = 0.6\delta$ for $x = 3\delta$ (left) and $x = 5\delta$ (right).

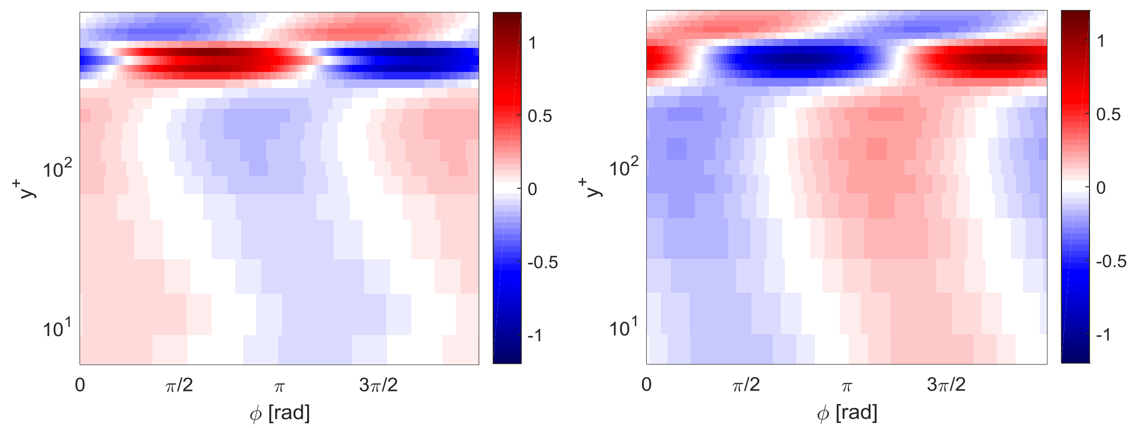

Figure 5. Phase mappings of modal velocity at $x = 3\delta$ (left) and $x = 5\delta$ (right)

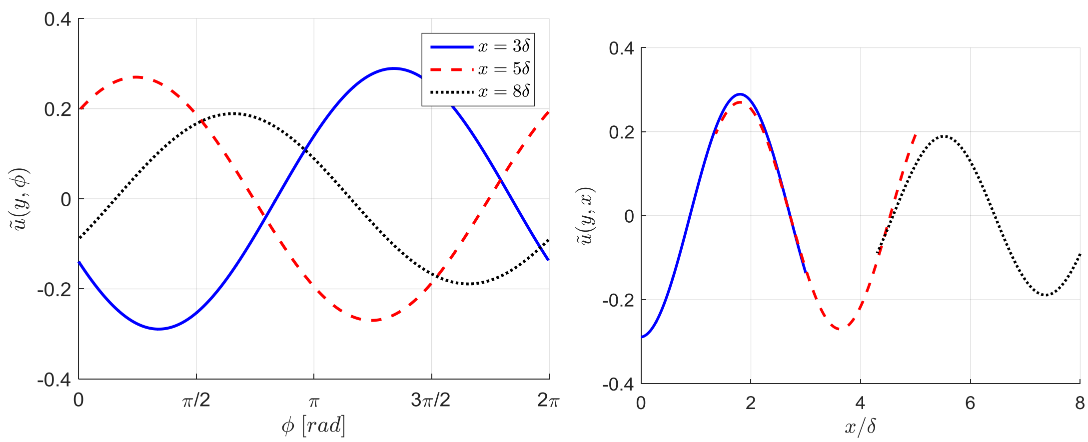

Figure 6. Modal velocity at $y = 0.6\delta$ for three measurement locations plotted as a function of phase (left) and as a function of pseudo-space, defined in Eq. (6) (right)

The modal component of velocity is well defined at the actuator height for all measurement locations. We expect to see a continuous modal velocity signal if we properly time-shift the modal velocity measured at each location. In Figure 6, right, the components of modal velocity have been aligned through a pseudo-spatial coordinate to match at the zero-crossings, enforcing the expectation of continuity across all measurement locations using the definition for x described in Equation 6. Here x is the streamwise pseudo-spatial coordinate, x_{meas} is the measurement location, and U_c is an appropriate convective velocity for the actuator location.

$$x = x_{meas} - \frac{\varphi}{2\pi} \frac{1}{f_p} U_c \tag{6}$$

The appropriate convective velocity for each streamwise location was found by adjusting the value to achieve the continuous modal velocity at zero crossings, shown in Figure 6, right. The values of the corresponding time crossings for each streamwise location are plotted in Figure 7, left. While the convective velocity is not necessarily constant moving downstream, we will assume that the overall convective speed is constant. A linear fit, shown as a dashed line in Figure 7, left, was used to compute the convective speed, and the value for the convective speed was found to be approximately $U_c = 6.2\ m/s\ or\ U_c^+ = 20$. The convective velocity has been plotted with the canonical mean and the plasma-on wake profile in Figure 7, right to show that it lies between the two profiles as expected for a typical convective velocity.

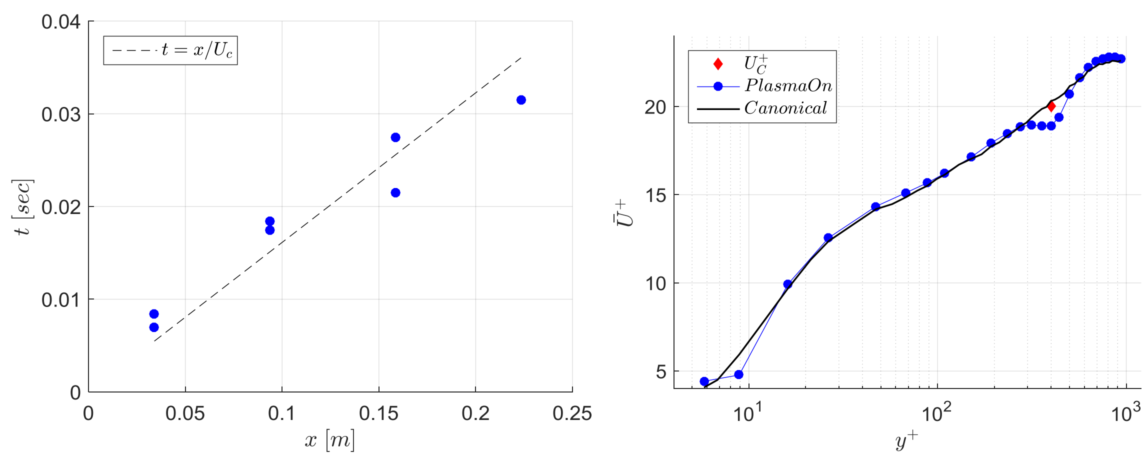

Figure 7. Left: Times of zero-crossings and position extracted from the zero-crossings of modal velocity at $y = 0.6\delta$. Right: mean velocity profiles with the convective velocity plotted for reference.

Assuming that the residual turbulence at the actuator height also convects at the estimated convective velocity, the phase-locked analysis can be presented relative to the time when the large-scale structure passes a given streamwise location. In this case, we can properly compare phase-locked results at different streamwise locations.

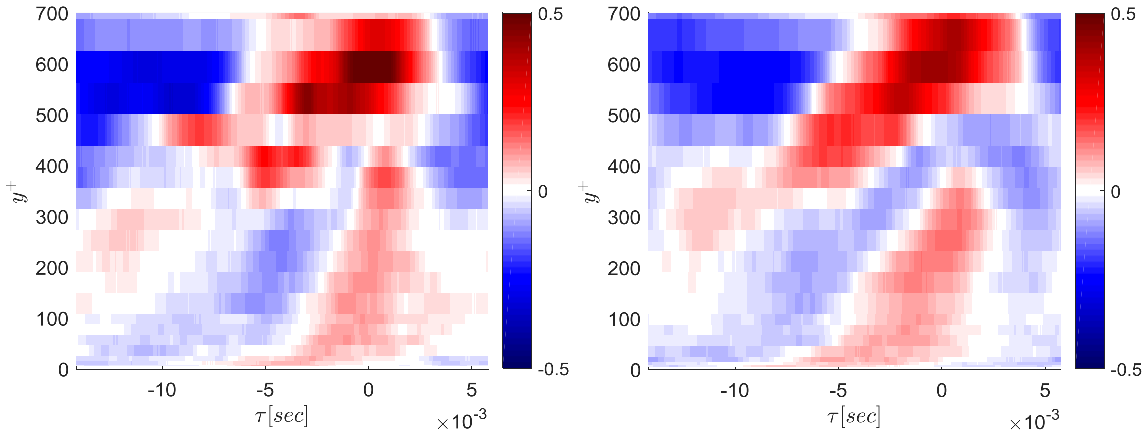

Figure 8. Maps of residual turbulence at x = 3δ (left) and x = 5δ (right) aligned by the time delay τ from when the LSS convects through the measurement location

The time-delay maps of the residual turbulence at two actuator locations of x = 3δ and 5δ are presented in Figure 8. In Figure 8 we see near-wall regions of turbulence that have been modulated by large-scale motions convecting in the wake region. These modulated regions extend from the wall through the log-region and lie directly below the peaks in residual turbulence seen convecting downstream which are generated by the actuator. It is also easy to make a direct comparison between the residual turbulence at different measurement locations when the plots are aligned by the time it takes the LSS to convect past the measurement location. We can see that the region of modulated turbulence and the turbulence generated by the actuator are changing in shape and extent as they move downstream. In Figure 9 the local maxima of the modulated turbulence near the wall at three measurement locations have been marked to give an indication of the angular inclination of these near-wall structures. Near the wall the modulated turbulence does not have a linear shape but as it extends into the log region, the shape becomes approximately linear. Using these local maxima the angular inclination of the structures from the wall and width of these structures can be estimated. Defining an accurate and repeatable measure of these quantities is difficult in this experiment, but in general it is clear that the modulated structures are stretching and becoming less inclined with the wall as they move downstream. We expect that this behavior will continue until it reaches some limit further downstream and continues asymptotically or dissipates. For the canonical TBL at large Reynolds numbers, a natural large-scale structure has an inclination of about 15 degrees [1] and our furthest downstream location has an inclination on the order of 20 degrees. This suggests that even 8δ from the trailing edge of the actuator the flow is still adjusting to the synthetic large-scale structure.

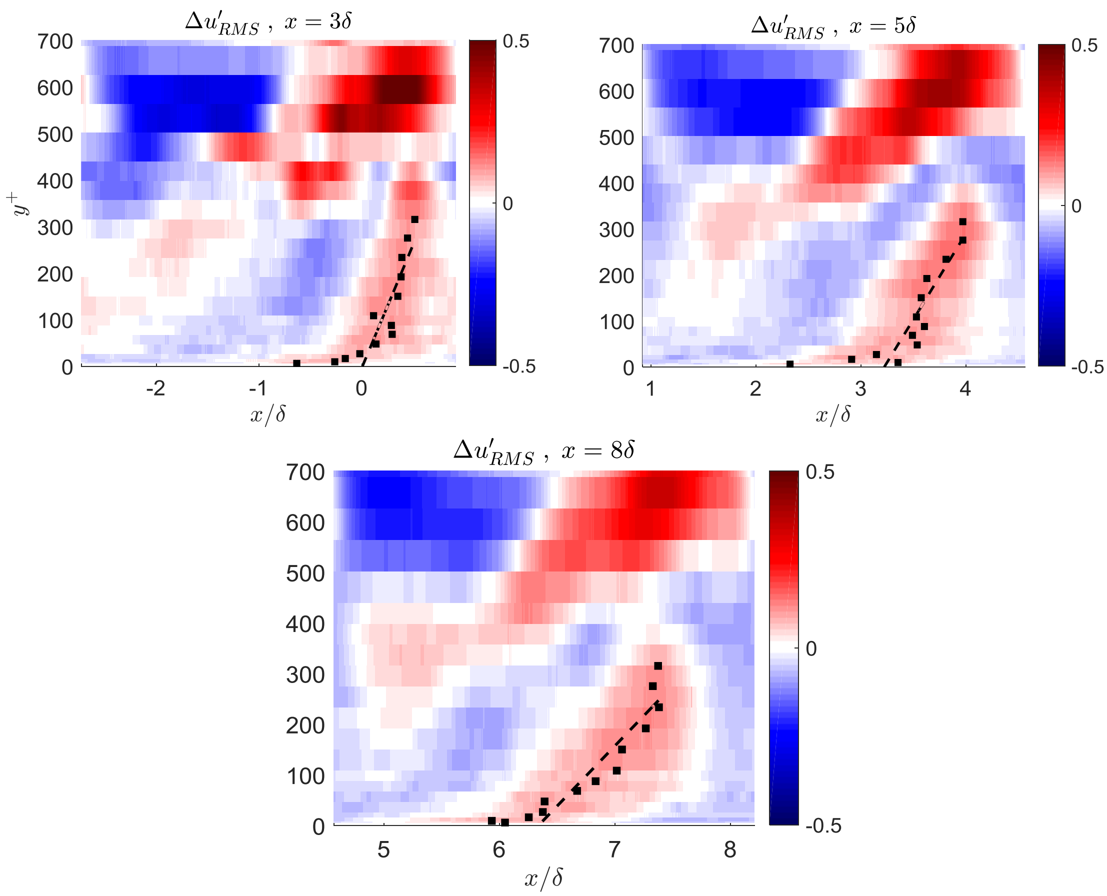

Figure 9. Aligned pseudo-spatial maps of residual turbulence with the maxima of the amplified turbulence near the wall marked to show inclination and extent of structures for $x = 3\delta$ (top left) $x = 5\delta$ (top right) and $x = 8\delta$ (bottom)

A natural extension of the pseudo-spatial coordinate described in Equation 6 is that the flow field downstream of the actuator can be reconstructed by combining together quantities from the individual measurement locations. By interpolating the overlapping areas, this combining technique gives a continuous snapshot of the flow field where the size of the large-scale synthetic structure can be measured and the evolution of the modulated near-wall turbulence can be seen simultaneously at different streamwise locations. The pseudo-spatial reconstruction of modal velocity and residual turbulence are presented in Figure 10.

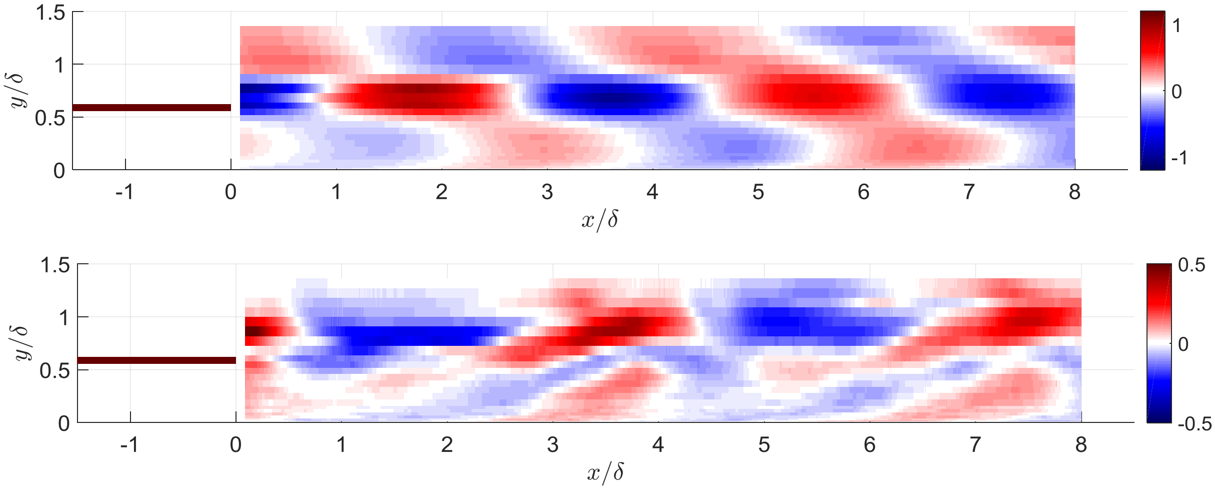

Figure 10. Pseudo-spatial reconstruction of the residual turbulence field (bottom) and the modal velocity field (top) normalized by u_τ

In addition to qualitatively analyzing the shape of the modulated near-wall turbulence, additional methods can be used to quantify the interaction of the near-wall turbulence and convecting large-scale motions. Quasi-steady theory [14] states that the changes in residual turbulence should change linearly with the slow changes in the modal velocity. In Figure 11, right, the modal velocity and residual turbulence have been normalized by the respective mean quantities at the specified wall normal location and plotted together showing qualitatively that as the modal velocity changes, so does the residual turbulence, though it is not an exactly linear response. If we compare all measurement locations, Figure 11 left, we can see that the response of the near-wall turbulence to the modal velocity is becoming more linear as you move downstream.

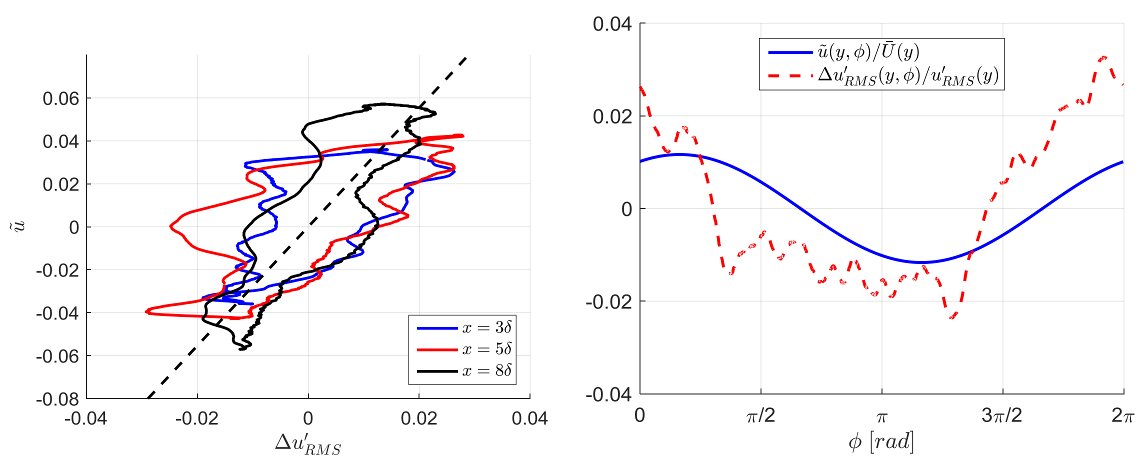

Figure 11. Left: Modal velocity versus residual turbulence at different streamwise locations. The dashed line is the linear fit for the quantities at $x = 8\delta$. Right: components plotted separately to demonstrate an approximate linear response at $y^+ = 15$.

In addition to analyzing the phase-locked results, there have been several modulation coefficients defined below that quantify the correlation of the near-wall small-scale fluctuations and large-scale fluctuations. These modulation coefficients have been calculated using Equations 7 and 8, respectively, and the results are presented in Figure 12. In the so called Φ-coefficient [9] the small-scale motions are represented by the changes in residual turbulence which, due to phase locked analysis will only include triadic interactions of scales that are multiples of the scale defined by the plasma forcing frequency. In the so called Ψ-coefficient [15] the small-scale motions are being represented by the envelope of small-scale fluctuations which are defined by a prescribed cut-off scale. The cutoff is determined by analyzing the scale separation in the premultipled spectra and for this experiment the cut-off was $\lambda^+ = 2000$, though the separation region between scales in this experiment is very narrow, see [11] for details. The low-pass filtering of small-scale fluctuations means that the Ψ-coefficient considers triadic interactions of all scales below the cutoff. This is the important difference in the modulation coefficients as the large-scale motions in both cases are represented by the modal velocity component or the change in velocity being generated at exactly the actuator forcing frequency.

$$\phi(y) = \frac{\langle \tilde{u}(y,\varphi) \Delta u'_{rms}(y,\varphi) \rangle_\varphi}{\sqrt{\langle \tilde{u}(y,\varphi)^2 \rangle_\varphi} \sqrt{\langle \Delta u'_{rms}(y,\varphi)^2 \rangle_\varphi}} \tag{7}$$

$$\Psi(y) = \frac{\langle \tilde{u}(y,\varphi) E(u_s^2) \rangle_\varphi}{\sqrt{\langle \tilde{u}(y,\varphi)^2 \rangle_\varphi} \sqrt{\langle E(u_s^2)^2 \rangle_\varphi}} \tag{8}$$

The modulation coefficients look very similar in shape for both cases and at all measurement locations. Near the wall the modulation coefficients are both nearly one indicating that there is a strong correlation between the large and small-scale motions at y-locations near the wall. Above the geometric center of the log-region the modulation coefficients cross through zero, and the large and the small scales become negatively correlated. At the actuator location these modulation coefficients return to positive values and quickly become negative again directly above the actuator due to the wake dynamics in the immediate area downstream of the actuator. In the outer region, the modulation coefficients become positive again due to the intermittency effects of the boundary layer interface. Looking at the changes in the coefficients with the streamwise location, it again becomes evident that the further downstream the large-scale structure have convected, the more correlated near-wall turbulence becomes with the synthetic structure. While either of these coefficients may be appropriate to use, the Φ-coefficient is particularly useful in this experiment because it directly compares the relevant quantities, such as the modal velocity and residual turbulence and is defined by a strong phase reference instead of a prescribed scale cutoff, needed to compute Ψ-coefficient.

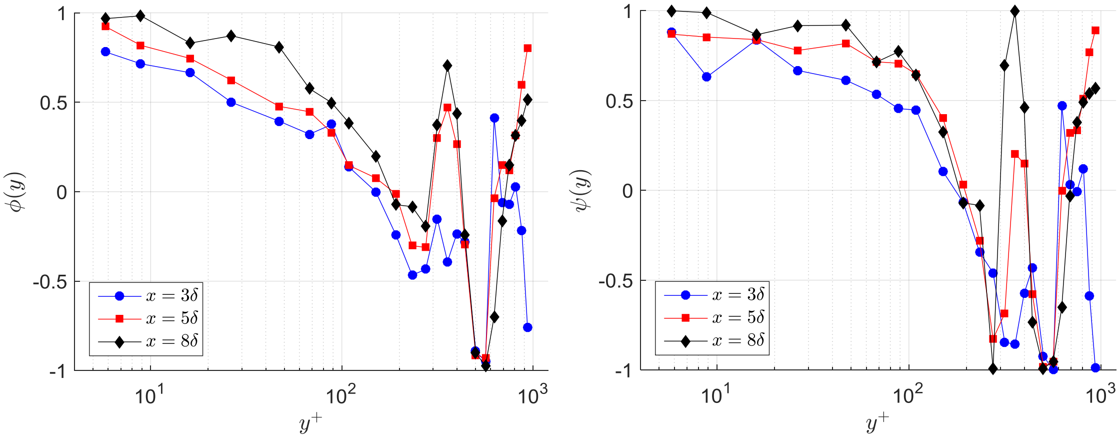

Figure 12. (left) Φ-modulation coefficient at all streamwise measurement locations. (right) Ψ-modulation coefficient at all streamwise measurement locations.

V. Conclusions and Future Work

From the results presented above it has been shown that synthetic large-scale motions can be effectively introduced inside of a low Reynolds number boundary layer using periodic plasma actuation to mimic the dynamics of a higher Reynolds number boundary layer. The structures produced by the actuator modulate turbulent structures near the wall and in the log-region of the boundary layer. These regions of modulated turbulence occur directly below peaks in residual turbulence generated by the plasma actuator as they convect downstream. It has also been shown that there is a transient effect where the near-wall flow response to the large-scale motions becomes more strongly correlated. The near-wall modulated regions also change in shape and angular orientation as they convect downstream, widening and becoming less inclined with the wall. The modulation effect suggests that when synthetic large-scale motions are introduced into the boundary layer there will be a measurable change in relevant flow parameters such as drag as a result.

In future experiments, we will investigate the effect of the plasma actuator geometry, placement in the wall-normal direction and forcing frequency to see how these parameters effect the near wall turbulence. Preliminary results have already shown that there is a frequency or range of frequencies that will produce a maximum modulation near the wall for the given actuator configuration. Future experiments will also utilize PIV and wall-mounted sensors to measure additional velocity components and instantaneous shear stress at the wall as well as obtain time resolved measurements of the full 2D flow field at once. One of the unique features of the current experiment is that in a low Reynolds number boundary layer there is no peak of coherent large-scale motion in the outer region of the boundary layer. If we performed the same experiment in a high Reynolds number boundary layer, we would no longer be adding a synthetic large-scale structure to the boundary layer, but rather modifying the large-scale structure that naturally exists in TBL. This type of experiment could provide a better understanding of the boundary layer dynamics at Reynolds numbers more relevant to modern turbulence problems.

Acknowledgements

This work is supported by Office of Naval Research, Grant number N00014-18-1-2534. The U.S. Government is authorized to reproduce and distribute reprints for governmental purposes notwithstanding any copyright notation thereon.

References

[1] M Guala, SE Hommema, RJ Adrian, "Large-scale and very-large-scale motions in turbulent pipe flow," J. Fluid Mech., 554, pp. 521-542, 2006.

[2] Mathis, R., Hutchins N., and Marusic, I., "Large-scale Amplitude Modulation of the Small-scale Structures in Turbulent Boundary Layers." Journal of Fluid Mechanics. 628 (2009): 311-336.

[3] N. Hutchins and I. Marusic, "Large-scale influences in near-wall turbulence," Phil. Trans. R. Soc. A, 365, pp. 647–664, 2007.

[4] R. Mathis, N. Hutchins, and I. Marusic, "A predictive inner–outer model for streamwise turbulence statistics in wall-bounded flows," J. Fluid Mech., 681, pp. 537–566, 2011.

[5] Adrian, R. J., Meinhart, C. D. and Tomkins, C. D., "Vortex organization in the outer region of the turbulent boundary layer," J. Fluid Mech., 422, pp. 1-53, 2000.

[6] de Silva, C. M., Hutchins, N. & Marusic, I., "Uniform momentum zones in turbulent boundary layers," J. Fluid Mech., 786, pp. 309-331, 2016.

[7] D.M. Schatzman, and F.O. Thomas, "An experimental investigation of an unsteady adverse pressure gradient turbulent boundary layer: embedded shear layer scaling," J. Fluid Mech., 815, pp. 592–642, 2017.

[8] Computation of Turbulent Boundary Layers--1968 AFOSR-IFP-Stanford Conference: Compiled data. Editors: D. E. Coles and E. A. Hirst, Thermosciences Division, Stanford University, 1969.

[9] P. Ranade, S. Duvvuri, B. McKeon, S. Gordeyev, K. Christensen, and E.J. Jumper, " Turbulence Amplitude Amplification in an Externally Forced, Subsonic Turbulent Boundary Layer", AIAA Journal, 57(9), pp. 3838-3850, 2019.

[10] Duvvuri, S., and McKeon, B., "Phase relations in a forced turbulent boundary layer: implications for modelling of high Reynolds number wall turbulence". Philos Trans A Math Phys Eng Sci., 375(2089), 20160080, 2017.

[11] Lozier, M. Midya, S. Thomas, F. O. Gordeyev, S. "Experimental Studies of Boundary Layer Dynamics Using Active Flow Control of Large-Scale Structures", Paper 5B-3, 11th International Symposium on Turbulence and Shear Flow Phenomena (TSFP-11), 2019.

[12] Thomas, F. O., Corke, T. C., Iqbal, M., Kozlov, A. and Schatzman, D., "Optimization of SDBD Plasma Actuators for Active Aerodynamic Flow Control" AIAA Journal, Vol. 47, No. 9, pp. 2169-2178, 2009.

[13] Klewicki, J., Fife, P., Wei, T. and McMurtry, P., "A physical model of the turbulent boundary layer consonant with mean momentum balance structure", Phil. Trans. R. Soc. Lond. A, 365, pp. 823–840, 2007.

[14] Zhang, C. Chernyshenko, S. I. "Quasisteady quasihomogeneous description of the scale interactions in near-wall turbulence", Phys. Rev. Fluids 1, 014401, 2016.

[15] Duvvuri, S., and McKeon, B.J., "Triadic Scale Interactions in a Turbulent Boundary Layer." Journal of Fluid Mechanics. 767, R4, 2015.